

γ production and neutron inelastic scattering cross sections for ^{76}Ge C. Rouki,^{1,*} A. R. Domula,² J. C. Drohé,¹ A. J. Koning,³ A. J. M. Plompen,^{1,†} and K. Zuber²¹European Commission, Joint Research Centre, Institute for Reference Materials and Measurements, Retieseweg 111, B-2440 Geel, Belgium²Technische Universität Dresden, Institut für Kern- und Teilchenphysik, Zellescher Weg 19, 01069 Dresden, Germany³Nuclear Research and Consultancy Group NRG, P. O. Box, 1755 ZG Petten, The Netherlands

(Received 31 July 2013; published 19 November 2013)

The 2040.7-keV γ ray from the 69th excited state of ^{76}Ge was investigated in the interest of Ge-based double- β -decay experiments like the Germanium Detector Array (GERDA) experiment. The predicted transition could interfere with valid $0\nu\beta\beta$ events at 2039.0 keV, creating false signals in large-volume ^{76}Ge enriched detectors. The measurement was performed with the Gamma Array for Inelastic Neutron Scattering (GAINS) at the Geel Electron Linear Accelerator (GELINA) white neutron source, using the $(n,n'\gamma)$ technique and focusing on the strongest γ rays originating from the level. Upper limits obtained for the production cross section of the 2040.7-keV γ ray showed no possible influence on GERDA data. Additional analysis of the data yielded high-resolution cross sections for the low-lying states of ^{76}Ge and related γ rays, improving the accuracy and extending existing data for five transitions and five levels. The inelastic scattering cross section for ^{76}Ge was determined for incident neutron energies up to 2.23 MeV, significantly increasing the energy range for which experimental data are available. Comparisons with model calculations using the TALYS code are presented indicating that accounting for the recently established asymmetric rotor structure should lead to an improved description of the data.

DOI: [10.1103/PhysRevC.88.054613](https://doi.org/10.1103/PhysRevC.88.054613)

PACS number(s): 25.40.Fq, 28.20.-v, 29.30.Kv, 29.40.-n

I. INTRODUCTION

Neutrinoless double- β decay ($0\nu\beta\beta$), a process that converts two neutrons (protons) into two protons (neutrons) with the emission of two electrons (positrons) only, is a subject under extensive investigation, due to its importance in understanding the nature of the neutrino, exploring physics beyond the standard model [1]. Due to its very long expected half-life (10^{25} y), the many experiments exploring $0\nu\beta\beta$ need to achieve a significant level of sensitivity, which involves setups with very large detector volumes and the simultaneous elimination of background events. One of the most promising emitters is ^{76}Ge , used in experiments like MAJORANA [2] and the Germanium Detector Array (GERDA) experiment [3], the latter located at Laboratori Nazionali del Gran Sasso (LNGS) in Italy. Germanium is a standard choice for a semiconductor detector material, since it can be produced in large sizes and offers high energy resolution and excellent efficiency. In double- β decay searches such detectors are enriched in ^{76}Ge as they serve also as the source (source equal detector approach). A potentially dangerous background component in the use of ^{76}Ge enriched detectors for $0\nu\beta\beta$ experiments is the occurrence of a γ ray with an energy of $E_\gamma = 2040.7$ keV from the decay of the 69th excited state of ^{76}Ge at 3951.9 keV (Table I). This γ ray can create an artificial signal very close to the energy where valid $0\nu\beta\beta$ events are expected (2039.0 keV) and can easily interfere with the measurements. For this reason, it is critical to have a reliable evaluation of the magnitude of this signal, which requires accurate measurements for the production cross section of the 2040.7-keV γ ray. Furthermore,

double- β searches into low-lying excited states, like the first 0^+ and 2^+ state, might also suffer from background due to inelastic neutron scattering. The $0\nu\beta\beta$ decay to the first excited state (2^+) is followed by a transition emitting a γ ray with an energy of $E_\gamma = 559.1$ keV. An additional γ ray with the energy $E_\gamma = 563.2$ keV occurs by $0\nu\beta\beta$ decay to the second excited state (0^+). Both lines have a full or partial overlap with the γ ray of the energy $E_\gamma = 562.9$ keV, emitted from the decay of the first excited state of ^{76}Ge . The first excited state of ^{76}Ge is readily excited by inelastic scattering of fast neutrons that may be present and the potential contribution to the background needs to be investigated. Neutron inelastic scattering was first identified as a potential source of background by Mei and Hime [4]. Subsequently, Refs. [5–7] reported on possible backgrounds due to neutron inelastic scattering on lead, germanium, iron, silicon, magnesium, and carbon with signatures similar to those of $0\nu\beta\beta$ decay of ^{76}Ge and ^{130}Te . The current experiment aimed to measure the 2040.7-keV transition of ^{76}Ge with the Gamma Array for Inelastic Neutron Scattering (GAINS) at the Geel Electron Linear Accelerator (GELINA), developed with the purpose of accurately determining cross sections with the $(n,n'\gamma)$ technique [8,9]. Because the production rate of the γ in question was anticipated to be very low, the effort was focused on the observation and measurement of the 3951.9-keV level of ^{76}Ge and its strongest transitions (Table I). There is a remarkable shortage in the literature regarding inelastic neutron scattering data for ^{76}Ge , even for the low-lying states and related γ emission. The excitation functions included in ENDF/B-VII.0 [11] are mainly based on calculations and the few available experimental data sets [12–16] involve considerable uncertainties. In particular, γ emission from the first excited state of ^{76}Ge (562.9 keV) was measured for incident neutron energies up to 2.43 MeV by Barry [13] and Lister and Smith [12] with uncertainties of 25 and

*Corresponding author: C. Rouki, haroularouki@gmail.com†Corresponding author: A. Plompen, arjan.plompen@ec.europa.eu

TABLE I. γ 's associated with the 69th level of ^{76}Ge [10].

E_γ (keV)	I_γ (%)
1259.5(5)	7(2)
2040.70(25)	8(2)
2843.50(9)	38(2)
3388.75(12)	67(4)
3951.70(14)	100(8)

30%, respectively. The excitation function of the 562.9-keV level up to 870 keV was determined by Konobeevskiy *et al.* [15] with similar uncertainties. The measurements of Chung *et al.* [14] achieved excellent accuracies of 10% for the excitation functions of the two lowest states and the associated γ 's however, only three incident neutron energies were investigated at 1.75, 2.13, and 2.55 MeV. Sigaud *et al.* [16] determined differential γ -ray production cross sections determined with a germanium detector at 55° in the energy range from 2 to 4.1 MeV with about 10% uncertainty. In this paper we compare with those data multiplied by 4π to compare with our angle-integrated γ production cross sections, a procedure which may lead to a bias of the order of the stated uncertainties.

Germanium is the construction material for active volumes of HPGe detectors and a main constituent of many other devices often operated in neutron fields. In addition to the significance of germanium as standard detector material, the accuracy of ^{76}Ge neutron data can affect the outcome of both experimental work and computer simulations. For this reason it is important to increase the volume and reduce the uncertainties of the existing experimental data points. In spite of the low statistics and practical limitations of the present work, the methodology used at GAINS allows the production of high accuracy measurements with the added advantage of high energy resolution provided by the use of a white neutron source. Therefore the low energy level information contained in the current data was also analyzed, and cross sections for γ , level, and inelastic scattering cross sections for ^{76}Ge were determined. Model calculations with the TALYS code [17] are compared with the data to investigate the impact of different physical choices and the reliability of estimates of cross sections beyond the range of the measurements.

II. EXPERIMENTAL DETAILS

The present data were collected at the Institute for Reference Materials and Measurements (IRMM) with the GAINS setup [8], developed to produce high-resolution (about 1 keV at neutron energy 1 MeV) inelastic scattering data and described extensively in several publications [8,9,18]. The setup is installed at flight path 3 of the GELINA facility at 198.8 m from the neutron source, which was operated at a 800-Hz repetition rate. The final configuration of the GAINS spectrometer consists of 12 large volume HPGe Canberra detectors in angles of 110° , 125° , and 150° to the beam, with four detectors positioned at each angle at distances of 16 to 18.6 cm from the target. For the current measurement

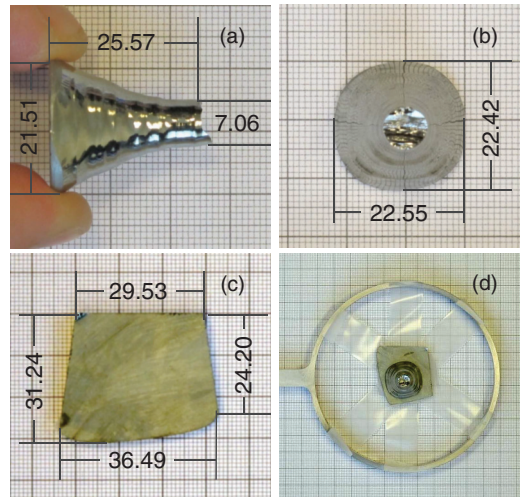


FIG. 1. (Color online) Side (a) and top (b) views of sample 1, sample 2 (c), and the two samples together (d) in the configuration in which they were irradiated (sample 1 facing upstream). The indicated measurements are in mm.

only the eight detectors positioned at 110° and 150° were used. The normalization of the measurements is provided by a ^{235}U fission chamber located 146.8 cm upstream from the target as described in Refs. [8,19,20]. For the present measurement the total data taking time was 165 h. Two ^{76}Ge enriched samples were used: sample 1, provided by TU-Dresden, was a monocrystal germanium slab of roughly conical shape [Figs. 1(a) and 1(b)] enriched to 87.44% (Table II). Sample 2, supplied by IRMM, had a quadrilateral shape and average thickness of 0.353 cm [Fig. 1(c)]. The isotopic ratios stated in Table II are derived from combining the values of Ref. [15] with mass spectrometry of the GeO_2 powder before reduction and zone refinement. The masses of the samples were measured as 14.56(1) g and 17.43(1) g, respectively. The two pieces were attached together at the target position to increase the available amount of material [Fig. 1(d)]. A measurement of sample 2 on a low-background HPGe detector before the irradiation showed that no γ -emitting impurities could be detected. A measurement of sample 2 on another low-background HPGe detector at IRMM, 1 day after the irradiation, showed that no activation products resulted from the experiment.

TABLE II. Isotopic abundances (%) in natural Ge and in the enriched material of the samples.

Isotope	$^{\text{nat}}\text{Ge}$	Sample 1	Sample 2
^{70}Ge	21.23(4)	0.001	0
^{72}Ge	27.66(3)	0.027	0.03
^{73}Ge	7.73(1)	0.110	0.13
^{74}Ge	35.94(2)	10.350	12.3(3)
^{76}Ge	7.44(2)	87.44(6)	87(1)

III. DATA ANALYSIS

The data analysis procedure followed to obtain γ production, level, and inelastic cross sections from GAINS data is detailed in Ref. [8], while recent revisions and new features incorporated in the methodology are described in Refs. [19,20]. Briefly, the primary measured quantity is the differential γ production cross section, described by Eq. (1) for detector j at angle θ_i and neutron energy E_k ,

$$\frac{d\sigma_j}{d\Omega}(\theta_i, E_k) = \frac{1}{4\pi} \frac{Y_j(E_k)}{Y_{FC}(E_k)} \frac{\epsilon_{FC}\sigma_U(E_k)}{\epsilon_j} \frac{t_U}{t_s} \frac{A_s}{A_U} \frac{1}{c_{ms}(E_k)}. \quad (1)$$

In Eq. (1) j refers to the γ detector, FC to the fission chamber, U to the ^{235}U contained in the fission chamber, and s to the sample. The quantity Y_i is the net peak yield of the examined γ ray, Y_{FC} the fission chamber yield, ϵ the absolute detection efficiency, t the thickness (mass per area), and A the atomic mass number. The standard neutron-induced fission cross section of ^{235}U $\sigma_U(E_k)$ is obtained from Ref. [21] and $c_{ms}(E_k)$ is the correction factor for neutron multiple scattering. The angle-integrated γ production cross section for n detectors at angle θ_i is

$$\sigma(E_k) = 2\pi \sum_{i=1}^2 \frac{w_i}{n_i} \sum_{j=1}^{n_i} \frac{d\sigma_j}{d\Omega}(\theta_i, E_k) \quad (2)$$

and the angle integration coefficients w_i are 0.6957 for 150° and 1.3043 for 110° , which are the two angles used in this experiment. Using the notation $\sigma_\gamma(L_i \rightarrow L_j)$ for a γ emitted from the transition between levels L_i and L_j , the deexcitation of level L_i and its feeding from higher states determines the level cross section,

$$\sigma_{L_i}(E) = \frac{\sigma_\gamma(E, L_i \rightarrow L_j)}{p_\gamma(L_i \rightarrow L_j)} - \sum_{\substack{E_x(L_j) \leq E \\ j>i}} \sigma_\gamma(E, L_j \rightarrow L_i) \frac{p(L_j \rightarrow L_i)}{p_\gamma(L_j \rightarrow L_i)} \quad (3)$$

where E is the incident neutron energy in the center of mass, E_x the excitation energy, while $p(L_i \rightarrow L_j)$ and $p_\gamma(L_i \rightarrow L_j)$ are, respectively, the total (γ and internal conversion) and γ -ray emission probabilities for the transition $L_i \rightarrow L_j$. Finally, the inelastic cross section is

$$\sigma_{\text{inl}}(E) = \sum_{i=1}^{E_x(L_i) \leq E} \sigma_\gamma(E, L_i \rightarrow L_j) \frac{p(L_i \rightarrow \text{g.s.})}{p_\gamma(L_i \rightarrow L_j)}. \quad (4)$$

The level and inelastic cross sections depend on the measured γ production cross sections and the level and decay data, here obtained from Ref. [10]. The maximum incident energy for which these cross sections can be determined depends on the number of γ rays which are observed in the experiment. Level cross sections with feeding missed by the experiment or the decay scheme will be overestimated. In contrast, the inelastic cross section will be underestimated in case no transitions are observed for levels that decay directly to the ground state. In this work we therefore limit the energies for which these cross sections are presented to the range where they can be relied on.

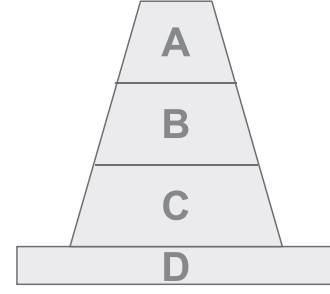


FIG. 2. The segmentation of the target in the MCNP5 simulations used to calculate the changes of the neutron reaction rate and γ attenuation in the volume of the target.

A. γ detector efficiency

The determination of the γ detection efficiency was performed by a method combining calibration measurements and Monte Carlo modeling, described in detail in Ref. [22]. The calibration measurements were taken with a ^{152}Eu point source for a total of 25560(1) s. The experimental efficiency for the extended sample ϵ_i was obtained from the expression

$$\epsilon_i(E_\gamma) = \epsilon_{\text{ext,calc}}(E_\gamma) \frac{\epsilon_{\text{point,meas}}(E_\gamma^{\text{Eu}})}{\epsilon_{\text{point,calc}}(E_\gamma^{\text{Eu}})}. \quad (5)$$

The ^{152}Eu γ 's at 444, 867, 1299, and 1408 keV were used to extrapolate to the γ energies of interest. The emission uncertainties of these γ 's range between 0.43 and 0.67%, making the total uncertainty associated with the source 0.8%. Taking into account the level of agreement between calculated and measured efficiencies, the overall uncertainties for the γ detection efficiency were between 1.5 and 1.7% (Table III).

In the MCNP5 [23] model used for the above calculations the Ge target was simulated with a homogenous and isotropic volumetric γ -emitting source comprising of two components: a truncated cone corresponding to sample 1 and a rectangular parallelepiped corresponding to sample 2. The same configuration was used in the calculation of the correction factors for neutron multiple scattering in the target and air attenuation of the beam. Due to the unusual shapes of the samples, the above calculations are approximate. First, the geometry that was realized in the calculations is more regular than the actual sample shape. Second, for a fraction of the incoming neutrons the sample is quite thick (near one scattering length) so the inelastic scattering rate is inhomogeneous, leading to an inhomogeneous γ source. As a result, the γ attenuation also is modified.

An estimation of these contributions was made using the following method. First, the variation of the neutron reaction rate was examined in increasing depths in the volume of the samples. For this purpose, the target in the MCNP5 model was divided in the four segments of Fig. 2, where the truncated cone is split in three sections of equal height (designated A–C in Fig. 2). The reaction rates were then calculated for each segment using the neutron energy distribution of the GELINA beam and the measured γ production cross section of the strongest examined transition (562.9 keV). The reaction rates per unit volume were found to be 26% (segment A),

TABLE III. Experimental γ detection efficiencies ϵ_i of the eight GAINS detectors for the investigated ^{76}Ge γ rays.

E_γ (keV)	Experimental efficiency ϵ_i ($\times 10^{-3}$)							
	Det. 1	Det. 2	Det. 3	Det. 4	Det. 9	Det. 10	Det. 11	Det. 12
562.9	3.83(6)	2.84(4)	3.07(5)	2.97(5)	3.14(5)	2.55(4)	3.06(5)	2.97(5)
545.5	3.89(6)	2.89(4)	3.12(5)	3.02(5)	3.19(5)	2.60(4)	3.11(5)	3.02(5)
847.2	3.15(5)	2.15(3)	2.46(4)	2.51(4)	2.61(4)	2.23(4)	2.48(4)	2.47(4)
431.0	4.39(7)	3.26(5)	3.50(5)	3.41(5)	3.59(5)	2.95(5)	3.51(5)	3.39(5)
1348.1	2.33(4)	1.73(3)	1.88(3)	1.89(3)	1.99(3)	1.69(3)	1.93(3)	1.89(3)
2040.7	1.52(2)	1.01(2)	1.28(2)	1.24(2)	1.21(2)	1.06(2)	1.30(2)	1.24(2)
3388.7	1.02(2)	0.67(1)	0.86(1)	0.83(1)	0.80(1)	0.70(1)	0.87(1)	0.83(1)
3951.7	0.88(1)	0.58(1)	0.74(1)	0.72(1)	0.70(1)	0.60(1)	0.76(1)	0.72(1)

25% (segment B), 24% (segment C), and 25% (segment D) of the total reaction rate in the target.

As a second step the γ -emitting source in the HPGe efficiency calculation model was divided in the same way, resulting in four isotropic sources for segments A–D of Fig. 2. The above reaction rate fractions were used to define the relative strength of each source. The γ detection efficiencies of the eight detectors was then calculated for the 562.9 keV γ ray and compared to the values of Table III. The results showed deviations between 0–8% with an average of 4%.

Finally, it is obvious from Fig. 1(d) that the samples were not precisely centered during the irradiation. This is expected to create asymmetry in the spatial distribution of the emitted γ 's and therefore variations between the γ -ray yields of detectors positioned at the same angle to the beam axis. A comparison of the γ -ray yields for each detector group, taking into account the efficiencies of Table III, displayed a consistent trend for all examined γ 's and a clear shift of the samples from the central target position towards the top left of the GAINS setup facing upstream. The effect was calculated for the 562.9-keV γ and gave standard deviations of 2–6% for the 110° detectors and 2–9% for the 150° detectors, averaging 4% in both groups.

The above contributions add up to 6% extra uncertainty on average in the γ detection efficiencies of the GAINS detectors. However, the calculations do not model the problem in full detail. Since individual detectors show excursions up to 10% for the source inhomogeneity effect in a symmetric sample as well as for the asymmetry effect, a conservative estimate of 10% uncertainty for the detection efficiency seems appropriate. This uncertainty was added to those given in Table III.

B. Fission chamber efficiency

The technique for the determination of the fission chamber efficiency has been detailed elsewhere [19,20,24,25]. The method is based on the rejection of the alpha peak from the amplitude spectrum with the application of a threshold in the center of the plateau that separates the alpha and fission fragment peaks. A flat or linear fit of the plateau region is then extrapolated to zero pulse height to calculate the total number of fissions. Further corrections are applied to account for the polarity effect [19] of the chamber, the number of fission fragments that stop in the deposit [26], and the inhomogeneity

of the UF_4 foils [27]. For the present measurement and the selected threshold the fission chamber efficiency was 82(1)%. Due to the limited data taking time of the current measurement and the resulting low statistics of the neutron yield distribution, the neutron pulse-height spectrum was normalized to an earlier measurement [20] with significantly better statistics. The normalization factor was calculated from the fission fragment integrals above threshold for the two pulse-height spectra.

C. γ production, level, and total inelastic cross sections

Well-defined peaks from all Ge isotopes of the target were identified in the γ pulse-height distributions. Specifically, for the most abundant isotopes ^{76}Ge and ^{74}Ge , the γ transitions from the first five levels were sufficiently strong to yield good statistics. None of the γ 's of Table I concerning level 69 were directly observable in the spectra.

In studying Ge isotopes using HPGe detectors, there is a risk of interference with γ 's created in the volume of the detectors by scattered neutrons. These are present to a degree in all HPGe spectra and display the characteristic sawtooth shape due to the sum of the full-energy peak and the recoiling Ge nucleus. Comparison with earlier GAINS measurements [20] showed a significant contribution from these γ 's to the strongest peaks of ^{74}Ge , which prohibited further work on this isotope. For the 847.2-keV peak of ^{76}Ge (1410.1 keV level) yields were extracted with some difficulty due to the tail of the 834.0-keV γ ray originating in ^{72}Ge inelastic scattering contained in the detectors. This affects the uncertainty especially close to threshold. Scattering contributions to the rest of the investigated ^{76}Ge lines [Fig. 3(a)] were negligible.

For the 3951.9-keV level the two strongest γ transitions were investigated ($E_\gamma = 3388.8$ keV, 3951.7 keV), as well as the 2040.7-keV γ ray in question [Fig. 3(b)]. The examined γ 's and associated levels are shown in Table IV and Fig. 3.

For the γ rays from low-lying levels the standard analysis procedure described in Ref. [8] was used following Eqs. (1) and (2). Corrections for neutron multiple scattering in the target and air attenuation effects were calculated with MCNP5 simulations according to the iterative procedure presented in Ref. [8], and good convergence was achieved in three iterations. Following scattering, the incident neutron loses energy by either elastic (a few percentages) or inelastic scattering or by the $(n,2n)$ process, where two lower-energy neutrons are created. These scattered neutrons [or the 2 $(n,2n)$ -neutrons] may interact with

TABLE IV. Examined γ 's from $^{76}\text{Ge}(n,n'\gamma)$ and associated initial (1) and final (2) levels [10,28].

E_γ (keV)	E_1 (keV)	$J_{\pi 1}$	E_2 (keV)	$J_{\pi 2}$	I_γ	γ -mult.
562.9	562.9	2 ⁺	0	0 ⁺	100	E2
545.5	1108.4	2 ⁺	562.9	2 ⁺	100	E2 + M1
847.2	1410.1	4 ⁺	526.9	2 ⁺	100	E2
431.0	1539.4	3 ⁺	1108.4	2 ⁺	65(7)	
1348.1	1911.0	0 ⁺	562.9	2 ⁺	100	
2040.7	3951.9	(1,2 ⁺)	1911.0	0 ⁺	8(2)	
3388.8	3951.9	(1,2 ⁺)	562.9	2 ⁺	67(4)	
3951.7	3951.9	(1,2 ⁺)	0	0 ⁺	100(8)	

the sample to produce the γ rays of interest, leading to a spurious additional yield. The multiple scattering correction factor removes this additional yield.

The γ production cross sections were then used to calculate the related excitation functions using Eq. (3) and level information from the evaluation of Singh [10] modified by the corrections given by Toh *et al.* [28]. From the known conversion coefficients the transition and γ -emission probabilities between two levels were determined, and from these the factors $p(L_j \rightarrow L_i)/p_\gamma(L_j \rightarrow L_i)$ of Eq. (3), which describe the contributions of the observed γ 's to each level (Table V). The results are detailed in Sec. IV A.

A more complex analysis was required for the 3951.9-keV level. Because of the anticipated small production cross section of the level, combined with the limited statistics, extremely low yields were expected for the involved γ 's and possible escape peaks. Therefore, although these lines were not immediately discernible, they could still be present in the spectra and concealed by the background.

To resolve this issue the yield of the HPGe detectors at the energies of Table I was investigated for neutron energies from just below the threshold and above. In the γ spectra for this energy range upper and lower limits were calculated for the positions where the peaks are expected as well as for adjacent regions defining the background. To this end first a detailed energy calibration was made for all detectors using ^{152}Eu measurements and 10 lines from the background and

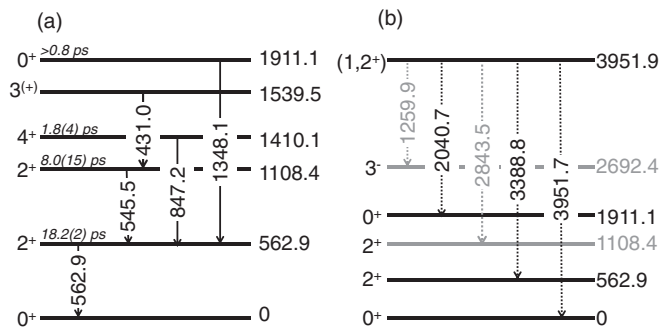


FIG. 3. Simplified partial level schemes of ^{76}Ge , displaying (a) the observed γ rays from the five lowest levels and (b) the γ 's originating in the 69th excited state at 3951.9 keV, according to Refs. [10,28]. The examined transitions and associated levels are displayed in black.

TABLE V. Contributing weights of the observed γ 's to the construction of the level cross sections.

γ ray	Ground state						
	562.9	1108.4	1410.1	1539.5	1911.1	3951.9	
562.9	1.000	1.000					
545.5	0.75(8)	-1.00(7)	1.68(7)				
847.2		-1.000		1.000			
431.0		-1.5(1)	-1.00(9)		2.5(2)		
1348.1		-1.000				1.000	
2040.7	13(3)	-8(2)	-5(1)		-1.0(3)	28(7)	
3388.8	1.5(1)	-1.00(8)	-0.57(5)		-0.12(3)	3.3(2)	
3951.7	1.000	-0.67(5)	-0.38(3)		-0.08(2)	2.2(1)	

^{76}Ge γ 's with energies between 431 and 2920 keV. The γ production cross sections were then determined according to the standard procedure described in Ref. [8]. The results are presented in Sec. IV B.

IV. RESULTS AND DISCUSSION

A. The low-lying states

Figures 4 and 5 show the angle-integrated γ production cross sections for the lower energy γ rays of Table IV. Existing data from Refs. [12–16] are also displayed for comparison.

For the 562.9-keV transition the measured distribution shows a slow increase between the threshold at 570.4 keV and 1 MeV and remains largely constant between 1 and 1.2 b. Some weak resonance structure is noticeable in the low energies. The measured cross sections have an average uncertainty of 12%, increasing significantly near threshold due to statistical fluctuations. The neutron energy spread ranges from 5 to 30 keV below 2 MeV to 80 to 140 keV between 2 and 3 MeV. Excellent agreement exists with the data sets of Barry [13] and Sigaud *et al.* [16], although there are considerable deviations from the former above 1700 keV. The author states an accuracy of around 25% for these measurements (not displayed in the figure). The results by Chung *et al.* [14] are within two standard deviations below our data. Significant differences exist with the cross sections of Lister and Smith [12], which increase rapidly below 1 MeV and extend between 1 and 2 b in the area

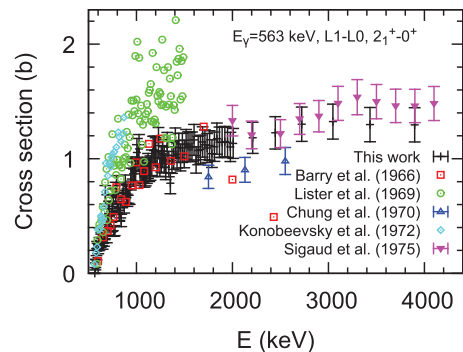


FIG. 4. (Color online) Measured angle-integrated γ production cross sections for the first excited state at 562.9-keV excitation energy in comparison with earlier data [12–16].

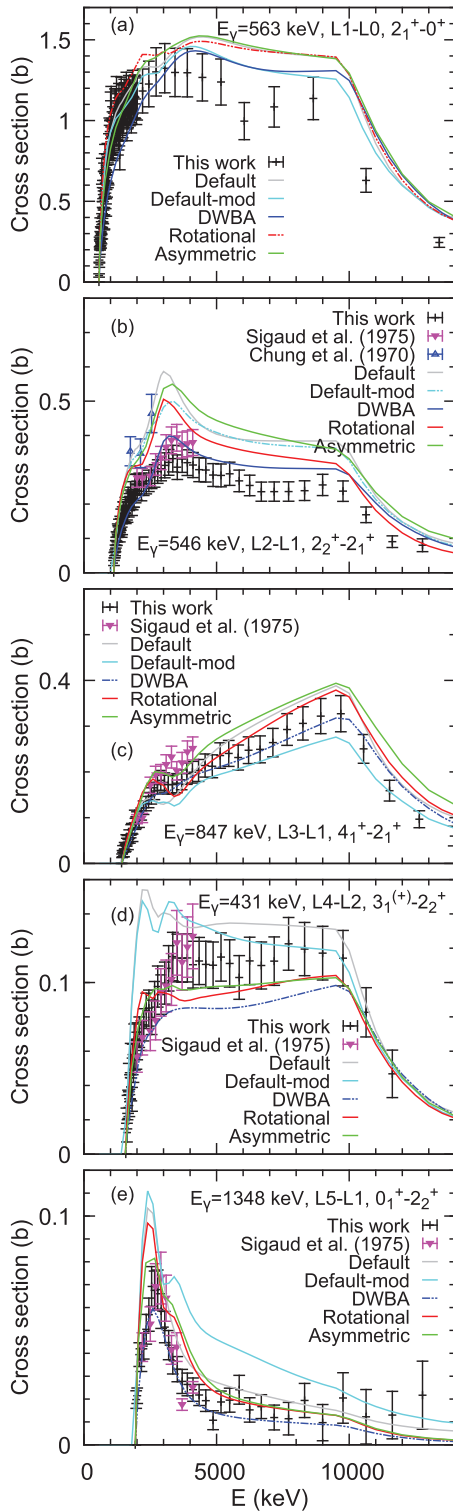


FIG. 5. (Color online) Measured angle-integrated γ production cross sections for the low-lying states of Table IV, in comparison with TALYS calculations and earlier data [14,16].

1–1.5 MeV. These values have a 30% uncertainty. The data of Konobeevskiy *et al.* [15] cover a smaller energy range and have a similar trend as those by Lister and Smith.

The 545.5-keV γ cross section [Fig. 5(b)] reaches 300 mb at 3 MeV and does not exceed that value for higher energies. The data have an average uncertainty of 12% and show reasonably good agreement with the data of Sigaud *et al.* [16], while the data by Chung *et al.* [14] are higher. The measured cross sections for the 847.2, 431.0, and 1348.1 keV γ rays have somewhat higher uncertainties (13–15%). It must be noted that a large fraction of the quoted uncertainties for the present results is related to the additional 10% uncertainty discussed in Sec. III A, connected with the irregular shape of the target. In all three cases the agreement with Sigaud *et al.* is excellent.

The resulting level excitation functions are shown in Fig. 6. The calculated cross sections are absolute only below the threshold of the first higher excited state that populates the level. Beyond that energy (2.69 MeV for level 1, 2.05 MeV for levels 2–4, and 3.07 MeV for level 5) the present data represent an upper limit.

The inelastic scattering cross sections (Fig. 7) are valid up to the threshold of the first level decaying to the ground state and which is not included in the measurement. This is 2.23 MeV. The uncertainties for the level excitation functions and the inelastic cross sections range from 15 to 20%. Finally, the present results for the total neutron inelastic cross section of ^{76}Ge (Fig. 7) have an average uncertainty of 15.7% in the examined energy range.

B. Comparison with model calculations

1. Model calculations

The new data for the low-lying states are compared with Hauser-Feshbach-Moldauer model calculations using the TALYS model code [17] to investigate the impact of different physical choices and comment on the reliability of estimates of cross sections on theoretical grounds beyond the range of the measurements. The first calculation is the so-called TALYS-default physical model which uses the Koning-Delaroche global optical potential [29], the Gilbert-Cameron level density model [30], Kopecky-Uhl γ strength functions [31], and the discrete level scheme reported in the Evaluated Nuclear Structure Data File (ENSDF) database up to the 40th excited level [10]. The structure of the first two excited states is taken into account using the distorted-wave Born approximation (DWBA). The parameter choices are documented in Ref. [17].

The default calculation assumes ^{76}Ge is a vibrational nucleus. However, it is now clearly established experimentally by Toh *et al.* [28], following up on a suggestion by Chou *et al.* [32], that ^{76}Ge should be considered as one of the exceptional nuclei with a stable asymmetric shape. To check for the impact of the structure of the nucleus on the cross sections, we made three additional calculations including four members of the ground-state band ($0^+, 2^+, 4^+, 6^+$) and four members of the γ band ($2^+, 3^+, 4^+, 5^+$) in coupled-channels calculations using the rotational model (labeled “Rotational”), the asymmetric rotor model (labeled “Asymmetric”), and by including these levels using only the distorted wave Born approximation (labeled “DWBA”). These calculations are compared with a modified default model (labeled “Default-mod”) for which only the optical potential was adapted to obtain better agreement

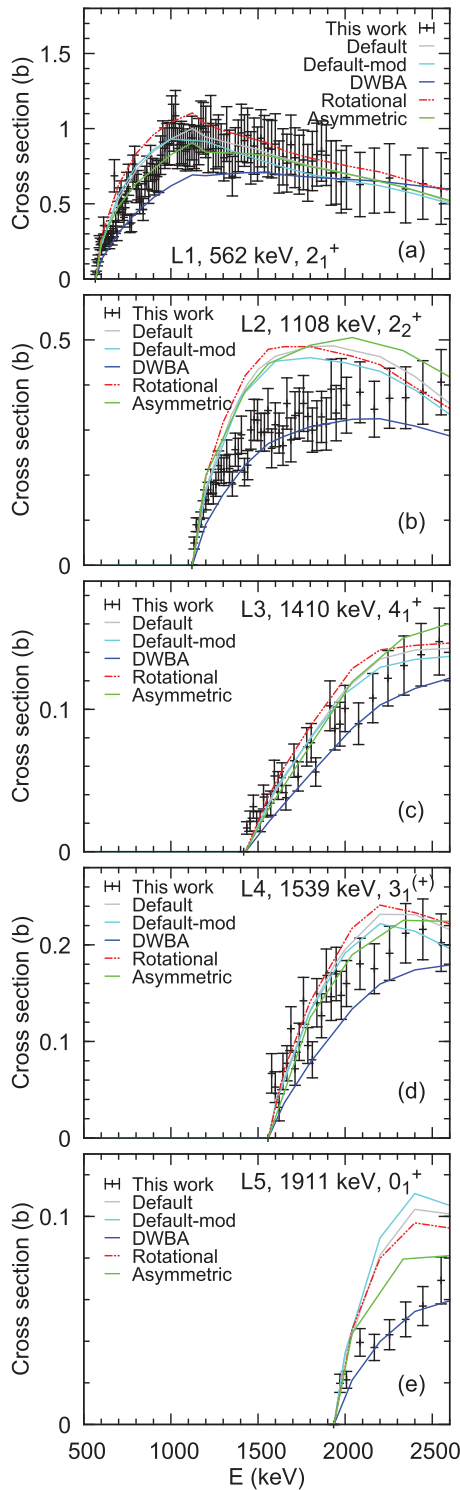


FIG. 6. (Color online) Excitation functions for the first five levels of ^{76}Ge compared with TALYS calculations.

with the data. The modified parameters with respect to the TALYS global potential are (modified/global) as follows: $E_F = -8.35/-7.75$ MeV, $r_V = 1.215/1.208$ fm, $a_V = 0.655/0.666$ fm, $v_1 = 54.6/54.2$ MeV, $d_2 = 0.0225/0.0218$ MeV, $w_1 = 13.8/13.5$ MeV, and $a_W = 0.485/0.558$ fm (E_F is the Fermi energy, r_V the radius parameter of the real volume potential,

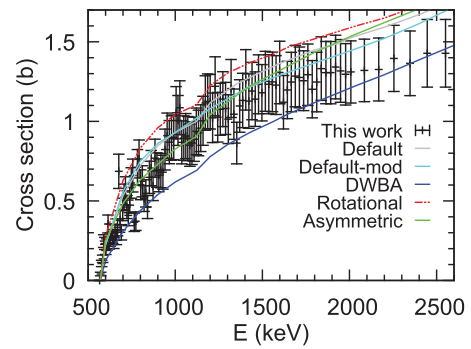


FIG. 7. (Color online) Measured inelastic scattering cross section for ^{76}Ge compared with TALYS results.

a_V its diffuseness and v_1 its first depth parameter, w_1 is the first depth parameter of the volume imaginary potential, d_2 concerns the imaginary surface potential, and a_W is their common diffuseness parameter [29]).

From the work of Toh *et al.* [28] it is further clear that (1) the level scheme in ENSDF is not complete even when only the first 40 levels are considered and (2) the ground-state band has a moment of inertia only about half that of a rigid rotor. Therefore all calculations shown here besides “Default” and “Default-mod” include a moment of inertia 50% of the rigid rotor value (spin cut-off parameter 0.5) in the level density model and limit the included discrete levels to the first 20. For these 20 levels the data available in ENSDF were modified to incorporate the results of Ref. [28]. This includes changes to the branching ratios for level 2 (1.108 MeV) and level 4 (1.539 MeV), two additional decay modes with branchings and an adjusted excitation energy for level 6 (2.022 MeV), an adjusted excitation energy, firm spin assignment (6^+) and established decay branch for level 9 (2.454 MeV), and a redefinition of level 10 (2.487 MeV, 5^+) with three identified decay branches.

Calculations with and without the adjusted spin cut-off parameters and with either 20 or 40 levels show no impact below a 3-MeV incident energy and no significant impact (changes within 5%) for the levels with spins up to 3 and their decay γ rays. For the levels with higher spins the cross sections increase in an energy-dependent way by at most 15%.

2. Comparison with the data

The only available total cross-section experiment for ^{76}Ge [33] (Fig. 8) agrees best with the coupled-channels calculations using the rotational model (deformation $\beta = 0.25$ [10]), but agreement is certainly also good for the default and modified default models. The changes going to the asymmetric rotor model or the DWBA are significant.

For the first level at 562.9 keV (Fig. 5) the γ production cross section is best described by the asymmetric rotational model up to about 4 MeV. This is confirmed by the level cross section and the inelastic cross section. However, in this energy range the rotational model and the default model with or without modified optical model potential are certainly also consistent with the data while the DWBA is below the data by at most two standard uncertainties. Above 4 MeV the “Default-mod” and the DWBA are consistent with the data, the

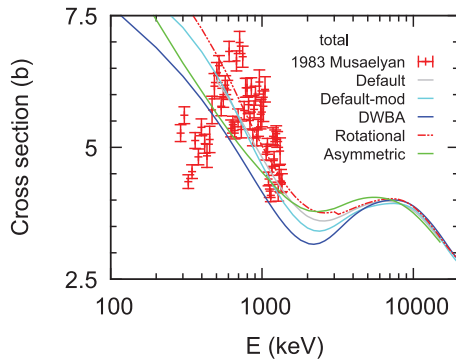


FIG. 8. (Color online) The available total cross section dataset for ^{76}Ge compared with TALYS calculations.

coupled-channels calculations being significantly higher than the data along with the default model. In agreement with the above, the level cross section (Fig. 6) below 2.5 MeV is well described by all approaches with a clear preference for the asymmetric rotor, the default, and the modified default calculations. The DWBA is low compared to the data around 1 MeV while the rotational model is on the high side. To the extent we can determine the total inelastic scattering cross section (up to 2.23 MeV) the conclusions for the first level translate one-to-one to this cross section.

For the second level at 1108 keV the γ production cross section (Fig. 5) for the 546-keV transition is significantly too high for all except the DWBA calculations. Also, for the level cross section (Fig. 6) below 2.5 MeV, agreement is best with the DWBA model.

For the third level at 1410 keV the γ production cross section for the 847-keV transition agrees well with the rotational model calculation and with the DWBA, while the default model and the asymmetric rotor model using the global potential are within two standard deviations ($E_n = 4\text{--}10$ MeV). The default model with modified potential is considerably lower than the default model remaining within two standard deviations below the data up to 10 MeV and in good agreement with the data above where the other calculations are high. The level cross section between threshold and 2.5 MeV is described by all calculations within the uncertainties.

For the 431-keV γ from level 4 at 1539 keV there is an obvious overshoot of the measured cross section by the default model and the modified default model in the first two MeV above threshold. Agreement is good for the other calculations with a slight preference for the asymmetric rotor model. In contrast with the γ production cross section, the level cross section for the first MeV above threshold shows good agreement with the cross sections of the default and modified default models. This suggests that the default and modified default models have a too-high feeding of this level by the decay of levels at higher excitation energy. Since this is not the same for the other calculations considered here, this must be related to the population cross sections of the higher-lying levels and not the γ -ray strength function or discrete level scheme which are common to all calculations.

For the 1348-keV transition from the fifth level at 1911 keV agreement is best with the DWBA while above the maximum

similar agreement is obtained using the default, rotational, and asymmetric rotor models. The behavior of the modified default model is peculiar at the higher energies. The level cross section confirms these findings. This 0^+ level is the only one studied in this work which is not part of the coupling scheme.

3. Summary of the model calculations

In conclusion, we have presented evidence that improvements over the default model are needed to obtain good agreement with the experimental γ production, level, and inelastic cross sections. In the present limited study, improvement is shown to be possible by considering the levels of the ground-state band and the γ band explicitly in either coupled-channels calculations with the rotational and asymmetric rotor model or in DWBA. In particular for the band head of the γ band ($E_x = 1108$ keV) agreement is best with the DWBA calculation. This seems to indicate that the collectivity of ^{76}Ge is weak. Agreement is also improved by modifying the optical potential but discrepancies remain for the head and second state of the γ band and the 0^+ level.

It must be noted that for firm conclusions the optical model should be optimized for each of the different approaches considered here and that this may only be done when adequate total cross-section data and, ideally, elastic scattering angular distribution data are available. At present there is insufficient experimental guidance to further pursue the study of the impact of nuclear structure on the cross sections by using empirical optical models. In such a situation, a natural alternative approach is to resort to calculations based on microscopic or semimicroscopic model ingredients. Earlier we have shown for ^{208}Pb and ^{209}Bi [34,35] that such an approach leads to very similar agreement with inelastic scattering data as the default model. We do not show it here but we have made similar calculations using the semimicroscopical approach. The total cross section agrees with the data equally well as the rotational and default models. However, also for all other cross sections the microscopic calculation is very similar to the default model and, hence, does not lead to the required improvement. Of course, also the microscopic calculation with TALYS does not take the structure of the states into account since it only concerns the optical potential, level densities, and strength functions and not yet the discrete level scheme.

We finally point out that for what is presented here the model approaches alternative to the default model indeed affect the direct reaction mechanism contribution (Fig. 9). A significant increase is seen for the modified optical potential in the whole energy range and for the DWBA below 7 MeV. For the rotational model the increase is significant only below 2 MeV, remaining well below the DWBA and modified potential. The asymmetric rotor even shows less direct contribution below 3 MeV, while rising above this energy to the level of the default potential. In contrast, the nonelastic cross section is strongly reduced compared to the default model in the DWBA. So the lower cross sections shown above for inelastic scattering in the DWBA are despite the increase of the direct contribution and are rather due to the decreasing nonelastic cross section, albeit with a larger fraction of the direct contribution. For the other calculations the nonelastic cross section is very

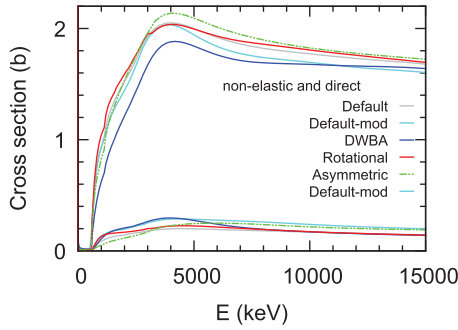


FIG. 9. (Color online) Direct (lower curves) and nonelastic (upper curves) cross sections for ^{76}Ge obtained with TALYS calculations.

similar to that of the default model up to 3 MeV. Above 5 MeV the modified potential is close the DWBA, while the coupled-channels calculations are closer to but somewhat above the default nonelastic cross section. It will be interesting to see how these effects are modified when the optical models for each of these cases are optimized. The need for better experimental data to allow improved modeling of these cases of interest to $0\nu\beta\beta$ studies was also found in Refs. [5,6].

C. The 3951.9-keV level

For the γ 's associated with the 3951.9-keV level the situation is shown in Fig. 10. The γ production cross sections have been plotted using uniform bin width on either side of the threshold (2–5 MeV) in order to evaluate possible variations and much broader bins in the high energies for a better assessment of general trends. In the case of the strongest 3951.7-keV transition [Fig. 10(a)] the distribution appears to rise above zero at the level threshold of 4003.9 keV. Beyond that energy it has an overall positive bias; however, negative values persist in the high energies even with very coarse binning. For the 3388.8-keV γ [Fig. 10(b)] a shift begins at threshold but towards negative values, and for the 2040.7-keV transition [Fig. 10(c)] a similar but stronger dip begins at about 3 MeV and appears to reach a minimum at threshold. Above threshold none of these γ rays show any significant positive trend, and on the whole these distributions are consistent with zero.

Consequently, the current results do not provide sufficient evidence of measurable cross sections for the studied transitions. Nevertheless, they can be used to define upper limits for the production of the 2040.7-keV γ ray under investigation and to draw some quantitative conclusions regarding potential interference with measurements of $0\nu\beta\beta$ events.

The definition of upper limits was made for broader energy intervals, selected to correspond to existing neutron flux measurements and calculations described in the next section (Table VIII). The production cross section σ_γ of the 2040.7-keV γ ray was determined from all three γ distributions independently according to the branching ratios of Table I. For each energy interval the most restrictive value of $\sigma_\gamma + 3u(\sigma_\gamma)$, where $u(\sigma_\gamma)$ is the uncertainty of σ_γ , was taken as the upper limit $\sigma_\gamma^{\text{UL}}$, corresponding to a confidence level of 99.7%. The results are presented in Table VI.

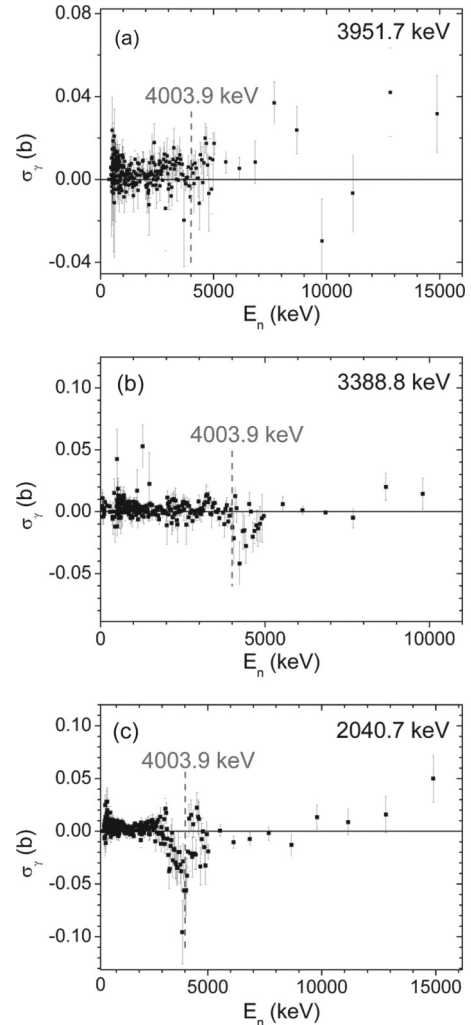


FIG. 10. Experimental results for the production cross sections of γ 's originating from the 3951.9-keV level of ^{76}Ge .

D. Implications for $0\nu\beta\beta$ studies

The obtained cross sections for the 2040.7-keV (upper limit) and the 562.63-keV γ rays may be used to determine their production rates (or an upper limit) in experiments targeting neutrinoless double- β decay of ^{76}Ge . It thus may be established if neutron-induced production of these γ rays is an important background component. Essential to such background estimates is the energy distribution and intensity of the fast neutron flux in the ^{76}Ge -based detectors of the experiments.

A systematic review of the neutron flux at LNGS is presented by Wulandari *et al.* in Ref. [36]. According to

TABLE VI. Upper limits for the production cross section of the 2040.7-keV γ ray, calculated at a 99.7% confidence level.

E_n^{min} (MeV)	E_n^{max} (MeV)	$\sigma_\gamma^{\text{UL}}$ (b)
4	5	0.0017
5	10	0.0014
10	15	0.0051

TABLE VII. The contributions of (α, n) reactions and spontaneous fission to the total neutron flux in Hall A of LNGS from the surrounding rock and dry concrete as estimated in Ref. [36].

	Rock ($n \text{ y}^{-1} \text{ g}^{-1}$)	Concrete ($n \text{ y}^{-1} \text{ g}^{-1}$)
(α, n)	4.4	0.51
Spontaneous fission	3.54	0.55

Ref. [36], the dominant sources of neutrons at LNGS are (α, n) reactions, induced by α particles from the decay chains of ^{235}U , ^{238}U , and ^{232}Th on light nuclei of the surrounding rock and concrete, and spontaneous fission of predominantly ^{238}U . Both processes give neutrons with energies up to about 10 MeV with the spontaneous fission contribution at about 30% at 1 MeV, reducing towards 10% at higher energies (Hall A). Estimates of their contributions to the total neutron flux are shown in Table VII. Higher-energy neutrons (up to 1 GeV) arise from muon interactions with the experimental environment. The cosmic ray-induced neutron background is 2 to 3 orders of magnitude lower [4] and can be considered negligible.

Quantitative estimates of the source term of the neutron flux thus depend on the uranium and thorium concentrations as well as on the composition of the surrounding rock, construction, and shielding materials. The latter also play an important role for the estimate of the flux in the ^{76}Ge -based detectors, as they modify the source spectrum by shielding and moderation.

Efficient background suppression is essential for all double- β -decay experiments and careful consideration has been given to the development of effective rejection strategies. Passive and active techniques employed by earlier setups like IGEX and the Heidelberg-Moscow experiment have achieved background rates of $0.06 \text{ counts keV}^{-1} \text{ kg}^{-1} \text{ y}^{-1}$ after the application of pulse-shape analysis [36]. GERDA aims to achieve levels between $10^{-3} \text{ counts keV}^{-1} \text{ kg}^{-1} \text{ y}^{-1}$ in the initial phases and $10^{-4} \text{ counts keV}^{-1} \text{ kg}^{-1} \text{ y}^{-1}$ in Phase III [37] with the combination of several background reduction methods like segmentation, pulse-shape analysis, ultrapure materials, and live and bulk shielding [38]. The substantial primary shield consists of a liquid argon cryostat of a 2-m radius enclosed within a water buffer with a thickness of up to 3 m. Basic simulations [39] indicate that the proposed configuration can effectively shield the detectors from external neutron flux. Possible internal contributions from detector components and the shielding itself will be minimized by the removal of most cladding and contact materials and the selection of radiologically clean materials, while an active system of Cerenkov counters is foreseen for muon rejection.

In the absence of neutron transport simulations for the complete GERDA setup and conclusive calculations of the neutron source term in the detectors, in the following we examine the extreme case of unshielded Ge detectors exposed directly to the external background of the LNGS experimental Hall A, as estimated in Ref. [36]. Our aim is to draw some quantitative conclusions on the possible interference from the ^{76}Ge γ 's directly valid for the GERDA experiment, which could be also applicable for similar deep underground measurements,

TABLE VIII. Neutron flux distributions in Hall A of LNGS from Refs. [42] and [36]. See the text for notation.

Neutron energy (MeV)		Neutron flux ($10^{-6} \text{ cm}^{-2} \text{ s}^{-1}$)		
E_n^{\min}	E_n^{\max}	(i)	(ii)	(iii)
2.5	5	0.18(4)	0.18(5)	0.12(4)
5	10	0.04(1)	0.05(2)	0.03(2)
10	15	0.0007(2)		

provided the thorium and uranium concentrations do not differ too much.

Reference [36] presents a systematic evaluation of six past neutron flux measurements undertaken at LNGS [39–45] and compares the experimental neutron spectra with results from Monte Carlo simulations, performed for different experimental halls and accounting for variations in rock composition and humidity of the concrete. For Hall A the result of Ref. [30] agrees with the calculations of the fast neutron flux ($E_n > 1 \text{ MeV}$), provided a choice is made for dry concrete. An accuracy of about 20% is claimed for both the measurement by Belli *et al.* [30] and the calculation of Wulandari *et al.* [36]; however, significant variability can be caused by humidity and the presence of equipment and materials in the hall. The obtained group fluxes $\phi_E(E_n)$, displayed in Table VIII, are designated as spectra (i), (ii), and (iii) for simplicity. Spectrum (i) refers to the measurement of Belli *et al.* [30] and corresponds to their most accurate result, based on a Watt fission spectrum for the displayed energy region. Spectra (ii) and (iii) refer to the Monte Carlo calculations of Ref. [36] for dry and wet¹ concrete, respectively.

Specific reaction rates R were calculated using the following expression:

$$R = n \sum_{n=1}^N \phi_E(E_n) \sigma(\gamma_i, E_n), \quad (6)$$

where n is the number of ^{76}Ge nuclides per unit mass of active detector material, N is the number of energy intervals considered, and $\sigma(\gamma_i, E_n)$ is the production cross section for the ^{76}Ge γ rays under investigation. For n both natural germanium and the ^{76}Ge -enriched material of the IGEX experiment are considered [46,47] (Table IX). The results, displayed in Table X and Table XI, represent the γ production rates in natural and enriched germanium exposed directly to the neutron flux in Hall A of LNGS. The estimates of Table XI and Table XII include the uncertainties in the measured γ -ray yields, the branching ratio data, and the flux spectrum but not the variability of the spectrum.

For comparison, assuming the Heidelberg-Moscow limit of $T_{1/2} > 1.9 \times 10^{25} \text{ y}$ [48], efficiency 95% [37], and the materials of Table IX, then the ^{76}Ge $0\nu\beta\beta$ peak at 2039 keV is expected to present event rates of $R_{2039 \text{ keV}} < 0.02 \text{ kg}^{-1} \text{ y}^{-1}$

¹The terms “dry” and “wet” concrete refer to water content of 8% and 16%, respectively, the maximum possible variations for the humidity of the concrete at LNGS [typical water content 12(4)%].

TABLE IX. Abundance and isotope density n_m for natural germanium ($^{\text{nat}}\text{Ge}$) and for the ^{76}Ge enriched ($^{\text{enr}}\text{Ge}$) detectors of the IGEX experiment [47].

Ge Isotope	$^{\text{nat}}\text{Ge}$		$^{\text{enr}}\text{Ge}$	
	Abundance (%)	n_m (g^{-1})	Abundance (%)	n_m (g^{-1})
70	21.23%	$1.76 \cdot 10^{21}$	0.005%	$3.98 \cdot 10^{17}$
72	27.66%	$2.29 \cdot 10^{21}$	0.005%	$3.98 \cdot 10^{17}$
73	7.73%	$6.41 \cdot 10^{20}$	0.050%	$3.98 \cdot 10^{18}$
74	35.94%	$2.98 \cdot 10^{21}$	12.510%	$9.95 \cdot 10^{20}$
76	7.44%	$6.17 \cdot 10^{20}$	87.430%	$6.95 \cdot 10^{21}$

for natural and $R_{2039 \text{ keV}} < 0.24 \text{ kg}^{-1} \text{ y}^{-1}$ for enriched Ge at a 90% confidence level.

Considering an energy resolution of 3.6 keV [37], the highest possible 2040.7-keV background (Table X) translates to $0.0227 \text{ counts keV}^{-1} \text{ kg}^{-1} \text{ y}^{-1}$ for bare detectors. In order to achieve the target background of $10^{-4} \text{ counts keV}^{-1} \text{ kg}^{-1} \text{ y}^{-1}$ as in GERDA Phase III, the foreseen shielding must reduce neutron flux in the detectors by a factor of 3. Taking into account that a 55- to 60-g cm^{-2} polyethylene layer is sufficient to reduce external neutron flux by six orders of magnitude [39], it is evident that the 2040.7-keV γ ray of ^{76}Ge is of no consequence for the GERDA experiment.

Other ^{76}Ge -based $0\nu\beta\beta$ setups, like the earlier Heidelberg-Moscow [48] and IGEX [47] experiments and the operating MAJORANA experiment [2], use considerably weaker primary shields based mainly on copper and lead. The current result can be used to estimate the shielding efficiency for these setups, as well as other Ge-based experiments that require high sensitivities, like dark matter searches.

Double- β decay to the 1122.3-keV excited 0^+ state deexcites by a $0^+ \rightarrow 2^+ \rightarrow 0^+$ chain, emitting two electrons with sum energy of 917 keV and two γ 's of 559.1 and 563.2 keV. The transition is expected to be produced with a ratio of $\Gamma_{0^+}/\Gamma_{\text{g.s.}} = 3.7910^{-3}$ to the ground state according to Ref. [49]. Assuming the above parameters, this implies event rates of $R_{1122 \text{ keV}} < 7.710^{-5} \text{ kg}^{-1} \text{ y}^{-1}$ for natural and $R_{1122 \text{ keV}} < 9.110^{-4} \text{ kg}^{-1} \text{ y}^{-1}$ for enriched Ge at a 90% confidence level. Comparing with the production rates of Table XI, the 562.9-keV γ ray from ^{76}Ge could be a serious problem for possible experiments targeting this particular state. The presence of neutrons can introduce further complications from

TABLE X. Production rates (upper limits in $10^{-3} \text{ kg}^{-1} \text{ y}^{-1}$, confidence level 99.7%) of the 2040.7-keV γ ray of ^{76}Ge in natural and enriched germanium in Hall A of LNGS, calculated with the neutron flux distributions (i)–(iii) of Table VIII.

ΔE_n (MeV)	$^{\text{nat}}\text{Ge}$			$^{\text{enr}}\text{Ge}$		
	(i)	(ii)	(iii)	(i)	(ii)	(iii)
2.5–5	3.88	4.27	3.11	43.76	48.13	35.01
5–10	1.90	2.98	2.44	21.41	33.64	27.52
10–15	0.13			1.46		
Total	5.91	7.25	5.55	66.62	81.77	62.53

TABLE XI. Cross section of the 562.9-keV γ ray and production rates in $\text{kg}^{-1} \text{ y}^{-1}$ in natural and enriched germanium in Hall A of LNGS for the neutron flux distributions of Table VIII.

ΔE_n (MeV)	σ_γ (b)	$^{\text{nat}}\text{Ge}$			$^{\text{enr}}\text{Ge}$		
		(i)	(ii)	(iii)	(i)	(ii)	(iii)
2.5–5	1.24(4)	4(1)	4(1)	3(1)	49(11)	49(14)	33(11)
5–10	1.11(4)	0.9(2)	1.1(4)	0.6(4)	10(2)	12(5)	7(5)
10–15	0.48(4)	0.007(2)			0.07(2)		
Total		5(1)	5(1)	4(1)	59(11)	61(15)	40(12)

the simple β decay of the intermediate nucleus ^{76}Se , which can be produced by successive (n, p) and (p, n) reactions. Both these sources of background can be minimized with adequate neutron flux suppression and can be entirely eliminated by the requirement of a triple coincidence between the electron sum energy and the two γ 's, as proposed in Ref. [49].

Finally, it should be clear that contributions to the background under the peaks of interest will be produced by inelastic scattering on levels with an excitation energy less than the 2039-keV $0\nu\beta\beta$ energy due to the sum energy of the emitted γ ray and that of the recoiling germanium. Of course, this requires a sufficiently high incident neutron energy, also because the ionization produced by the recoil is reduced by atomic collisions leading to phonons. The cross sections for the γ rays of the low-lying levels determined in this work will therefore help to establish a possible smooth background component when high-energy neutrons are present.

V. SUMMARY

The neutron inelastic scattering of ^{76}Ge was investigated with the GAINS setup at the GELINA time-of-flight facility. The work aimed at the observation and measurement of the 2040.7-keV γ ray originating in the 69th level of ^{76}Ge at 3951.9 keV. The transition is of interest for the GERDA experiment, researching neutrinoless double- β decay with large-volume ^{76}Ge enriched detectors. The strongest transitions of the level at 3951.7 and 3388.8 keV and the 2040.7-keV γ ray in question were examined. The results did not yield measurable cross sections and overall we cannot confirm that the population of the 3951.9-keV level was observed in the current measurement. An upper limit of 3 mb for the production cross section of the 2040.7-keV γ ray was determined.

The acquired data were also used to determine γ and level production cross sections for the low-lying states of ^{76}Ge , examining transitions from the first five excited states of ^{76}Ge . High-resolution distributions with uncertainties between 12 and 20% were produced, improving the accuracy of available data for this isotope. The inelastic cross section of ^{76}Ge was measured with an average uncertainty of 15.7% for incident neutron energies up to 2.23 MeV. These data add significantly to the available experimental information and will be of interest in estimating smooth contributions under the 2039-keV $0\nu\beta\beta$ peak for germanium detectors exposed to fast neutrons.

Nuclear model calculations were made using the state-of-the-art TALYS code and compared with the γ production and level excitation cross sections for the low-lying levels. The structure information provided by the recent experiment of Ref. [28] was used leading to improved agreement of the model calculations with experiment. The model calculations were hampered by a lack of total and elastic scattering cross sections for ^{76}Ge so no meaningful optical model optimization was possible. Therefore no positive confirmation

could be obtained for the stable asymmetric deformation of ^{76}Ge .

ACKNOWLEDGMENTS

We thank A. Caldwell, L. Bezrukov, and M. Hult for providing enriched ^{76}Ge samples and the GELINA staff for the experimental conditions. This work was supported by BMBF (05A08OD1, 02NUK013B).

-
- [1] S. Elliott and J. Engel, *J. Phys. G* **30**, R183 (2004).
 [2] N. Abgrall *et al.*, arXiv:1308.1633v1.
 [3] K. H. Ackermann *et al.*, *Eur. Phys. J. C* **73**, 2330 (2013).
 [4] D.-M. Mei and A. Hime, *Phys. Rev. D* **73**, 053004 (2006).
 [5] D. M. Mei *et al.*, *Phys. Rev. J. C* **77**, 054614 (2008).
 [6] V. E. Guiseppe *et al.*, *Phys. Rev. J. C* **79**, 054604 (2009).
 [7] A. Negret *et al.*, *Phys. Rev. J. C* **88**, 027601 (2013).
 [8] L. C. Mihailescu, L. Oláh, C. Borcea, and A. J. M. Plompen, *Nucl. Instrum. Methods A* **531**, 375 (2004).
 [9] L. C. Mihailescu, C. Borcea, and A. Plompen, *Nucl. Instrum. Methods A* **578**, 298 (2007).
 [10] B. Singh, *Nucl. Data Sheets* **74**, 63 (1995).
 [11] M. B. Chadwick, P. Obložinský, M. Herman *et al.*, *Nucl. Data Sheets* **107**, 2931 (2006).
 [12] D. Lister and A. B. Smith, *Phys. Rev.* **183**, 954 (1969).
 [13] J. F. Barry, *Supplement to the Proceedings of Conference on Nuclear Data - Microscopic Cross Sections and other Data Basic for Reactors, 17–21 October 1966, Paris, France* (IAEA, INDC/156, paper no. CN-23/59, 1967).
 [14] K. C. Chung *et al.*, *Phys. Rev. C* **2**, 139 (1970).
 [15] E. S. Konobeevskiy *et al.*, *Yad. Fyz.* **14**, 14 (1971).
 [16] J. Sigaud, Y. Patin, M. T. McEllistrem, G. Haouat, and J. Lachkar, in *Proceedings of the International Conference on Nuclear Cross Sections and Technology*, 3–7 March 1975, Washington, DC, USA (National Bureau of Standards, Washington, DC) Special Publication 425, Vol. II, p. 893.
 [17] A. Koning and D. Rochman, *Nucl. Data Sheets* **113**, 2841 (2012).
 [18] A. Negret, C. Borcea, J. Drohé, L. Mihailescu, A. J. M. Plompen, and R. Wynants, in *Proceedings of the International Conference on Nuclear Data for Science and Technology (ND2007), April 22–April 27, 2007, Nice, France* (EDP Sciences, Les Ulis, France, 2008).
 [19] A. Plompen, C. Borcea, D. Deleanu, P. Dessagne, M. Kerveno, M. Mosconi, N. Nankov, A. Negret, R. Nolte, C. Rouki *et al.*, *J. Korean Phys. Soc.* **59**, 1581 (2011).
 [20] C. Rouki, P. Archier, C. Borcea, C. De Saint Jean, J. Drohé, S. Kopecky, A. Moens, N. Nankov, A. Negret, G. Noguère *et al.*, *Nucl. Instrum. Methods A* **672**, 82 (2012).
 [21] A. D. Carlson, V. G. Pronyaev, D. L. Smith, N. M. Larson, C. Zhengpeng, G. M. Hale, F.-J. Hamsch, E. V. Gai, S.-Y. Oh, S. A. Badikov *et al.*, *Nucl. Data Sheets* **110**, 3215 (2009).
 [22] D. Deleanu, C. Borcea, P. Dessagne, M. Kerveno, A. Negret, A. J. M. Plompen, and J. C. Thiry, *Nucl. Instrum. Methods A* **624**, 130 (2010).
 [23] X-5 MonteCarloTeam, LANL Report No. LA-UR-03-1987, 2003 (revised 2005).
 [24] D. B. Gayther, *Metrologia* **27**, 221 (1990).
 [25] M. Mosconi, R. Nolte, A. Plompen, C. Rouki, M. Kerveno, P. Dessagne, and J. Thiry, *Proceedings of the Final Scientific EFNUDAT Workshop, 30 August–2 September 2010*, edited by E. Chiaveri (CERN, Geneva, Switzerland, 2010), p. 99.
 [26] Budtz-Jørgensen and H. Knitter, *Nucl. Instrum. Methods A* **236**, 630 (1985).
 [27] P. Schillebeeckx, A. Borella, J. Drohé, R. Eykens, S. Kopecky, C. Massimi, L. Mihailescu, A. Moens, M. Moxon, and R. Wynants, *Nucl. Instrum. Methods A* **613**, 378 (2010).
 [28] Y. Toh *et al.*, *Phys. Rev. C* **87**, 041304(R) (2013).
 [29] A. J. Koning and J. P. Delaroche, *Nucl. Phys. A* **713**, 231 (2003).
 [30] A. Gilbert and A. G. W. Cameron, *Can. J. Phys.* **43**, 1446 (1965).
 [31] J. Kopecky and M. Uhl, *Phys. Rev. C* **41**, 1941 (1990).
 [32] W.-T. Chou, D. S. Brenner, R. F. Casten, and R. L. Gill, *Phys. Rev. C* **47**, 157 (1993).
 [33] R. Musaelyan and V. Skorkin, *Proceedings of the 6th γ All-Union Conference on Neutron Physics*, 2–6 October 1983, Kiev, USSR (Neitronnaya Fizika, Moscow, CNIIatominform, 1984), Vol. 3, p. 162.
 [34] L. C. Mihailescu, C. Borcea, A. Koning, A. Pavlik, and A. J. M. Plompen, *Nucl. Phys. A* **799**, 1 (2008).
 [35] L. C. Mihailescu, C. Borcea, P. Baumann, P. Dessagne, E. Jericha, H. Karam, M. Kerveno, A. J. Koning, N. Leveque, A. Pavlik *et al.*, *Nucl. Phys. A* **811**, 1 (2008).
 [36] H. Wulandari, J. Jochum, W. Rau, and F. von Feilitzsch, *AstroP* **22**, 313 (2004).
 [37] I. Abt *et al.*, arXiv:hep-ex/0404039.
 [38] F. Avignone, S. Elliott, and J. Engel, *Revs. Mod. Phys.* **80**, 481 (2008).
 [39] V. Kudryavtsev, L. Pandola, and V. Tomasello, *Eur. Phys. J. A* **36**, 171 (2008).
 [40] R. Aleksan *et al.*, *Nucl. Instrum. Methods A* **274**, 203 (1989).
 [41] F. Arneodo *et al.*, *Il Nuovo Cimento A* **112**, 819 (1999).
 [42] P. Belli, R. Bernabei, S. D’Angelo, M. De Pascale, L. Paoluzi, and R. Santonico, *Il Nuovo Cimento A* **101**, 959 (1989).
 [43] E. Bellotti *et al.*, Laboratori Nazionali del Gran Sasso INFN Report No. INFN/TC-85/19 (1985).
 [44] M. Cribler *et al.*, *Astropart. Phys.* **4**, 23 (1995).
 [45] A. Rindi *et al.*, *Nucl. Instrum. Methods A* **272**, 871 (1988).
 [46] K. J. R. Rosman and P. D. P. Taylor, *Pure Appl. Chem.* **70**, 217 (1998).
 [47] C. Aalseth, F. Avignone III, R. Brodzinski, S. Cebrian, D. González, E. García, W. Hensley, I. Irastorza, I. Kirpichnikov, A. Klimenko *et al.*, *Phys. Atom. Nucl.* **63**, 1225 (2000).
 [48] H. Klapdor-Kleingrothaus, A. Dietz, L. Baudis, G. Heusser, I. Krivosheina, B. Majorovits, H. Paes, H. Strecker, V. Alexeev, A. Balysh *et al.*, *Eur. Phys. J. A* **12**, 147 (2001).
 [49] M. Duerr, M. Lindner, and K. Zuber, *Phys. Rev. D* **84**, 093004 (2011).